Journal of Membrane Science 684 (2023) 121847

Contents lists available at ScienceDirect

Journal of Membrane Science

journal homepage: www.elsevier.com/locate/memsci

Simultaneous measurement and ODE-modeling of ion- and water permeability through ion exchange membranes

Lars Varain [a,*], Silvia Larisegger [b], Michael Nelhiebel [b], Günter Fafilek [a]

[a] TU Wien, Institute of Chemical Technologies and Analytics, Getreidemarkt 9, AT-1060, Vienna, Austria
[b] KAI GmbH, Europastraße 8, AT-9524, Villach, Austria

ARTICLE INFO

Keywords:
ion diffusion
Osmosis
Simultaneous measurement
ODEs
Concentration cell

ABSTRACT

The determination of diffusion coefficients in solid materials as a measure of particle mobility is of great scientific interest. This applies both to desired diffusion, such as in fuel cell- and dialysis membranes, and to undesired diffusion in insulating materials. In any case, diffusion is a measure of performance. Especially for solvated ions, the permeability of the solvent must also be considered.

In this work, a measurement method for the simultaneous determination of coupled ion diffusion and water permeability in polymer membranes is presented. For this purpose, measurement methods for the determination of concentration-, volume- and membrane-potential changes are integrated into a single, miniaturized concentration cell.

A system of ordinary differential equations is developed for the general description of the coupled transport processes. This makes it possible to model the interdependent solute concentration and solvent volume changes. The coefficients of interest are defined by fitting the model parameters to the measured data.

To evaluate the new combined measurement setup, a freestanding ion exchange membrane with largely known properties is used. The membrane of choice is a Nafion® NR211 membrane, since Nafion® is one of the most investigated PEM in literature and allows a comparison of computational and experimental results with existing data.

1. Introduction

The usual applications for IEMs are membrane based separation processes and energy conversion and production. Common applications for IEM based separation processes are diffusion-dialysis and electrodialysis for waste water recovery [1,2] and for the food industry [3] as well as drinking water treatments [4]. The reverse electrodialysis, on the other hand, can be used to generate electrical energy from the membrane potentials of cells with alternating AEMs and CEMs which are fed with solutions of different salinity grades, such as river and ocean water [5], or even the salinity provided by human urine [6].

Depending on the application the main transport properties of such membranes are therefore the ion permeability, the ion selectivity, and the water permeability. Determining these properties is essential for the improvement of existing systems and development of new ones. A common way to do so, is to measure the time-dependent changes of the corresponding parameters in a concentration cell.

A concentration cell consist of two equally sized chambers, separated by the membrane of interest. The chambers are filled with electrolytic solutions of different concentration. Due to the concentration gradient the ions diffuse from the higher concentrated, through the membrane, to the lower concentrated side. From measured concentration change over time, on the lower concentrated side, the permeability and diffusion coefficient can be calculated. The accepted framework for transport processes involving aqueous electrolytes is the diffusion solution model [7–13]. It has the same form as Fick's law integrated over the membrane thickness, and also takes into account the sorption- or partitioning coefficient [7]. Therefore, the diffusion coefficients can be calculated as the quotient of the (measured) permeability coefficient and the partitioning coefficient.

The solution diffusion model is also applicable for water transport. In that case, the parameter to be measured over time has to be the volume, which change is driven by a pressure gradient.

Additionally, the ion specific transport phenomena can be measured in form of a membrane potential, from which the transport numbers and selectivity can be determined [14,15].

* Corresponding author.
E-mail address: lars.varain@tuwien.ac.at (L. Varain).

https://doi.org/10.1016/j.memsci.2023.121847
Received 13 March 2023; Received in revised form 9 June 2023; Accepted 11 June 2023
Available online 16 June 2023

The common method to determine the concentration change in such diffusion cell setups is by measuring the electrical conductivity of the solution, as it is done by others before [8–11,16]. The water permeability is often measured in an additional setup. An commonly used tool is a reverse osmosis setup that requires an externally applied pressure [9,17], or a permeation cell that measures the relative humidity on the dry receiver side of a double chamber cell [18], ASTM F1249. Osmosis driven water permeability can be measured directly in an extended concentration cell, by observing the volume change with help of the filling height [12,13].

To measure the membrane potential in a concentration cell, a commonly used electrolyte for this experiment is potassium chloride (*KCl*) solution, since both ions have almost similar apparent transport numbers in neutral environments [19]. To maintain constant values, the electrolyte holding compartments are often supplied by an electrolyte stream ([20,21]). The membrane potential is then determined by measuring the potential difference of two reference electrodes besides the membrane [22]. By using the same type of junction reference electrodes filled with the same concentrated electrolyte solution, the concentration dependent electrode potentials cancel each other out. If plain reversible electrodes are used, the concentration dependence of the electrode potentials has to be taken into account as well [23,24].

However, in the previously mentioned works only one method is used at a time. Either they are just interested in one specific phenomenon ([8,10,11,16,20]) or they used different setups for the individual measurements ([9,23]).

The few works, which measure osmotic volume change additional to ion transport, provide just fragmentary mathematical descriptions, since they assume a single sided constant concentration ([12]) or neglect it all ([13]).

Works, which offer detailed mathematical models, on the other hand, again using non-simultaneous methods for the ion diffusion and osmosis measurement. Fernández de Labastida et al. [25] for example are using a fast concentration step method for the non-stationary determination of the salt diffusion and an independent osmotic permeability measurement to obtain the data which is fitted to a mathematical model which includes salt diffusion as well as osmosis.

Often, however, the most detailed mathematical descriptions of transport processes in concentration cells are only theoretical. The Onsager reciprocal relations of membrane transport phenomena are often explained on the example of such diffusion or migration cells ([26]), whereas the combination of the related driving forces then again depend on the application (see Ref. [27]).

The work of Narebska et al. should also be mentioned here [28]. Narebska et al. have already carried out very extensive studies on IEMs in their earlier work, including pressure-driven volume flow and salt diffusion flow in addition to osmotic volume flow, electroosmotic volume flow, electrical conductivity and concentration potential.

This work presents a measurement method for the simultaneous determination of coupled ion diffusion and water permeability in polymer membranes. For this purpose, measurement methods for concentration-, volume- and membrane-potential changes are integrated into a single miniaturized concentration cell.

For the general description of the coupled transport processes, a system of ordinary differential equations (ODE) is developed. The ODE system describes the bilateral concentration changes in the concentration cell. The concentration changes depend on both, ion diffusion and volume change caused by osmosis.

The rate determining parameters for the ion- and water transport in the ODE model are adjusted to fit the modeled concentration and volume changes to the measurements. Thus, the actual transport coefficients D_s and P_w are determined.

The additional measurement of the membrane potential is done to determine the apparent transport numbers of the involved ions in the membrane.

An ion exchange membrane (IEM) will be used as model membranes to develop this method for the holistic determination of membrane transport parameters. The IEM is used because all transport phenomena mentioned before can be conveniently observed. In addition, the transport properties in particular have been described in many studies before [12,17,18,23,25].

The IEM of choice is Nafion® NR211. This membrane is preferred because it has the smallest thickness of all available Nafion® membranes. This should reduce the measurement duration since the permeability depends also on the thickness. Most of the research data concerning Nafion® and especially the transport coefficients, however, are mostly available for thicker types (N117, N112, N1110). Nevertheless, the values are taken for comparison and evaluation because the different thicknesses have just a scaling effect on the measurements.

2. Experimental

2.1. Materials

The used IEM is a Nafion® NR211 membrane. The specific properties, according to the data sheet [29], are a thickness of 25.4 μm, a (dry) basis weight of 50 g/m^2, water uptake of 50.0 ± 3.0 % and an available acid capacity of min. 0.92 meq/g also referenced as ion exchange capacity (IEC).

The used electrolyte solution is composed from ACS grade KCl (VWR Chemicals) and DI water.

Prior to the measurement, the membrane undergoes a preconditioning. During the preconditioning, the initially dry membrane is immersed in an equilibration solution and thereby is hydrated and takes up ions according to its partitioning coefficient. Further, an extensive preconditioning, with several renewals of the equilibration solution, leads to a conversion of the functional groups to the corresponding anion or cation form. Usually the preconditioning is made with a solution that corresponds to the measurement solution [12,20,23,25]. This is primarily done to define a stable start condition. This is also helpful with regards to a simulation of the system since it saves the effort of modelling the complex uptake and swelling processes.

After the preconditioning routines according to Refs. [30,31] the conversion of the sulfonic acid groups from the proton to sodium form and the salt (sodium chloride) uptake according to the partitioning coefficient are complete. While the adsorbed counter ion concentration is relatively independent from the surrounding concentration [32], the actual salt concentration depends on the surrounding concentration and the partioning coefficient. Similar procedures has also been reported applicable for other alkali metal ions as lithium and potassium [33–35].

Following the prior mentioned works, the membrane is preconditioned in a KCl solution. The solution has the same concentration as the solution in the lower concentrated side of the cell at the beginning of the measurement. The membrane is treated in this solution for 3 h at 80 °C. Then it is rinsed with DI water and stored in a fresh solution at stable laboratory ambient temperature of 21 °C for at least 24 h until usage.

2.2. Measurement setup

The presented cell consists of two individual cylindrical chambers with a cross-sectional area of 100 mm^2 which are milled into polycarbonate (PC) blocks with a size of 50 × 50 mm and a thickness of 10 mm, which leads to a total volume of 1 ml per chamber. Additionally, each block has three openings from the sides. Two of them have screw threads, allowing the filling of the cell and the closing with the suitable nylon screws. The opening also allow the application of the measurement electrodes. The third opening has a wider, cylindrical shape and is used for the filling level measurement. The assembling of the whole cell is done by stacking the two structured blocks and clamping the membrane of interest in between. Two additional, unstructured PC blocks are used to close the cell. Fig. 1 shows the cell parts and the stacking order.

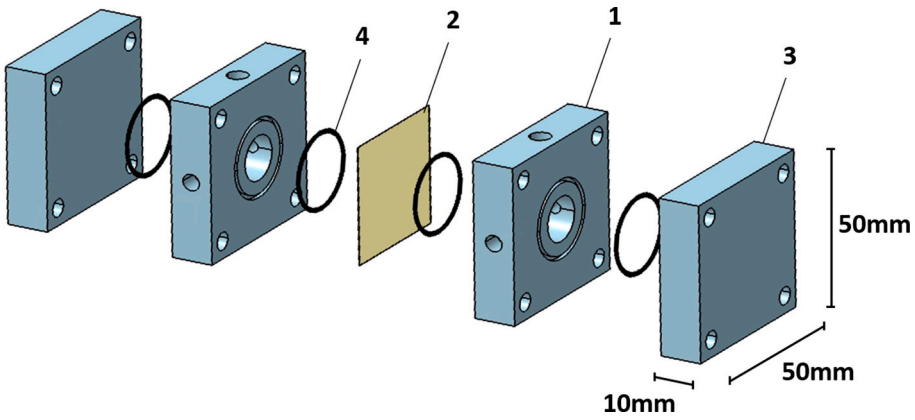

Fig. 1. Main components of the diffusion cell used in this work. (1) main elements made of polycarbonate blocks (50 × 50 × 10 mm^3), containing the electrolyte reservoirs (ø 11.28 mm) and three openings for filling, and applying devices. (2) Membrane under investigation, which is clamped between two main elements. (3) Cover plates made of polycarbonate to close the cell. (4) O-rings to seal the cell. The cell parts are held together by four bolts and appropriate nuts through the four holes located in the corner of each block.

The small volumes of 1 ml each has been chosen to measure the concentration- and membrane potential changes in reasonable time spans. For the additional measurement of the volume change, it is essential that the total volume remains constant. Therefore, the cell is designed as a concentration cell with stationary liquids rather than a flow-through cell.

In an unstirred solutions however, a stagnant solution layer is formed at the interface. With an assumed stagnant solution layer thickness of approximately 500 µm [26] and a diffusion coefficient of approx. 10^{-9} m^2/s for salt ions in water, the diffusion resistance of this layer is $0.5{\cdot}10^6$ s/m. The actual membrane resistance is presumable in the range of 10^7 s/m. Neglecting the concentration gradient in the solution would therewith lead to an error of 5%. The authors deliberately accept the deviations in order to be able to calculate with the metrologically accesible mass concentration in the following.

The measuring methods for the concentration change, the volume change and the membrane potential are all included in the one concentration cell. Fig. 2 a) shows a sketch of the cell including all used measurement adaptions and Fig. 2 b) shows a picture of a fully assembled cell.

The concentration change is measured on both sides, using electrical conductivity measurements. Therefore, one specially made conductivity measuring cell is used on each side, which fits into the miniaturized electrolyte chambers. Each cell is made from two 250 µm Pt wires, which are melted in a borosilicate glass double chamber capillary with a diameter of 2 mm and a length of 75 mm. Afterwards the outstanding ends are platinized to increase the surface (see Fig. 2 b)). The length of the outstanding ends is approximately 1 mm. Further, a specialized instrumentation setup is tailored.

Due to the extreme miniaturization of the EC-measuring cell, an exact calculation of a cell constant is not possible. That prevents the conductivity determination via a comparison to the standard literature reference values. Instead, reference measurements in the proposed working range are made for each individual µEC-cells, and the values between the reference measurements are interpolated by a second order polynomial. The measured conductivity values are then compared to the reference values by using a python/numpy script. Fig. 3 shows a sketch of the µEC-measurement setup and an exemplary reference curve.

The volume change is determined optically by monitoring the filling level. For this purpose, two floaters are developed which simplify the automated image processing, and which prevent an eventual drainage of the membrane. The floaters are made from polycarbonate tubes with a diameter of 7 mm and the volume is experimentally determined by adapting the length and therewith, the weight of the floater. The cylindrical opening in each chamber functions as a guidance for them. The quantitative level change is calculated from the heights of the floater via digital image processing. Basically, the image processing script is calculating the quantitative values by masking the floater and counting the pixel rows from the top down until the first pixel of the mask is found. The amount of pixel rows is then assigned to the corresponding reference value in ml. Fig. 4 shows the corresponding reference values. The reference value series is made by taking a specific amount of solution from one side of the cell via an Eppendorf pipette and fill it to the other side. The pictures taken with different reference filling levels are then evaluate by the mentioned digital image processing. The in-between values are interpolated by a first order polynom.

The membrane potential is determined by measuring the potential difference of two Ag/AgCl electrodes over the membrane. Since the electrodes are in direct contact to the chloride containing electrolytes of

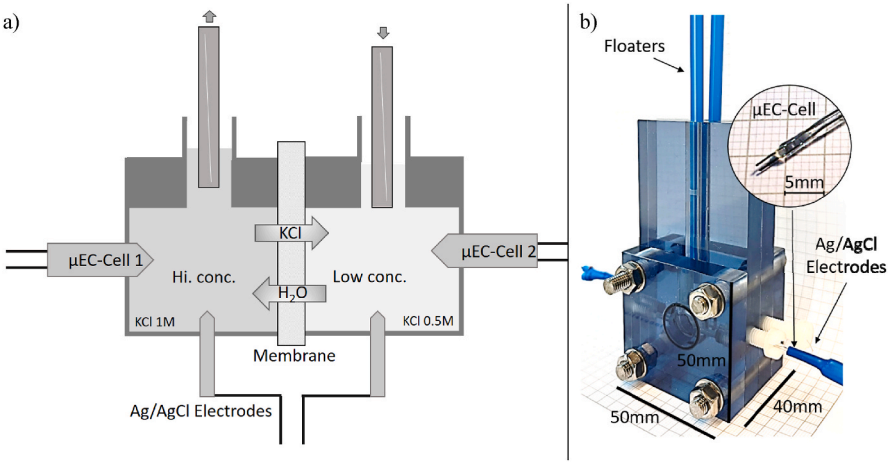

Fig. 2. a) Schematic of the complete measurement setup consisting of a concentration cell build from two chambers separated by the membrane of interest, two µEC-cells for measuring the concentrations in each chamber, two Ag/AgCl electrodes for potential difference measurments over the membrane and two floaters which positions are recorded via camera for volume change determination. The electrodes are connected to the corresponding measuring circuits over remote controlled reed switches to enable serial, pseudo parallel measurements. A PC is controlling the setup and records all data. b) Picture of a fully assembled cell. The height extension of the two main elements serve only the purpose of guiding the floaters. Additionally, a magnification of one of the used µEC-cell is shown, consisting of two platinized platinum wires melted into a double chamber capillary. The platinum wire diameter is 250 µm.

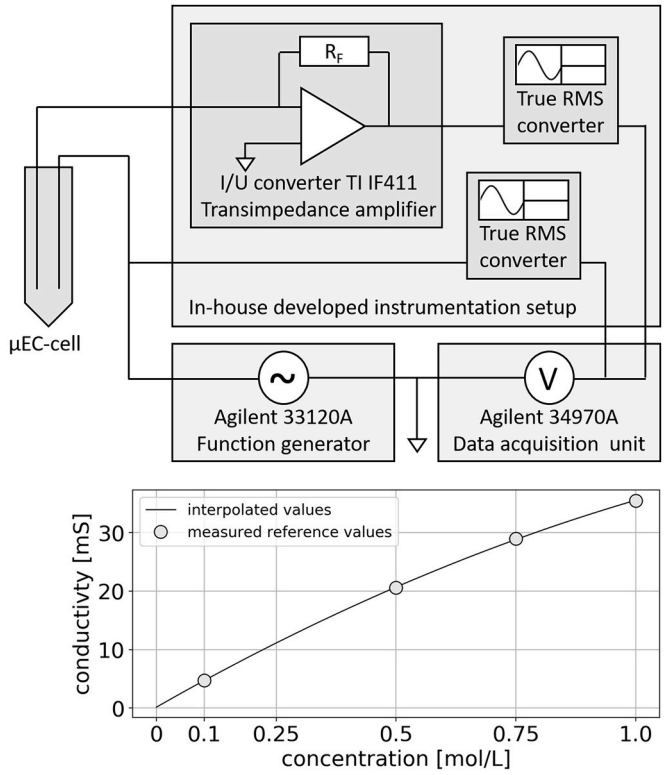

Fig. 3. Wiring scheme of the EC measurement setup with an Agilent 33120A function generator giving the input signal to the µEC-cell, an I/U converter as part of a zero resistance amperemeter (ZRA) converting the resulting current and an Agilent 34970A multichannel multimeter recording the true rms converted voltages. The lower graph shows an exemplary reference curve measured with the pictured setup (○).The in-between values are interpolated by a second order polynomial.

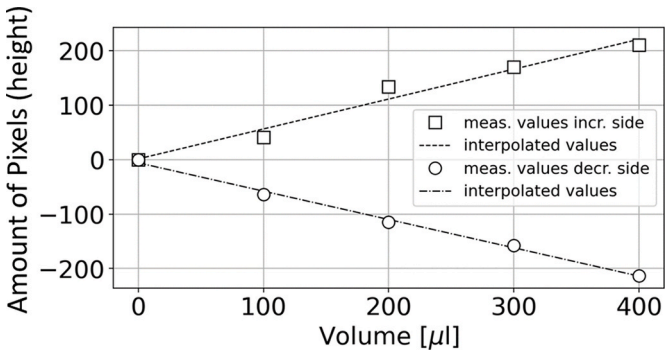

Fig. 4. Filling level reference values for the volume change determination. The reference value series is made by taking sequently 100 µl of solution from one side of the cell (○) via an Eppendorf pipette and fill it to the other side (□). The in-between values are interpolated by a first order polynomial.

different concentrations, the individual concentration dependent electrode potentials have to be considered as well. Further it is important to measure the potential difference currentless to prevent a galvanic loading of the electrodes. Therefore, an additional instrumentation amplifier with a high input resistance is used. The used amplifier is the *TI INA116* with an input resistance of 10^{15} Ω. The amplifier is wired as proposed in the datasheet, but with no additional amplification.

To verify the functionality of the measuring circuit and the *Ag/ AgCl* electrodes a series of test measurements is made. The test measurements are made with different concentrated KCl electrolytes in a beaker, in which the electrode potential are measured against each other. Even though, the electrode potentials should nominal be the same, there are some deviations of the measured values from the calculated ones. The offset range from 1.1 to 3.73 mV. This range could be explained by the response time of the electrodes which is needed to reach a stable equilibrium state after getting in contact with a new electrolytic surrounding. According to Brewer and Brown [36], "An explanation for the comparatively poor long term stability of the electrolytic type electrodes can be offered by considering the low geometric surface area and the exchange current density […]". Additionally an amplifier offset can be measured. The overall offset is knowingly accepted and can be count out during the evaluation of the measured values.

All measurements together are made in a pseudo parallel manner, to prevent interferences between the different electrodes (Ag/AgCl reference electrodes, EC measurement cells) and to minimize the amount of external measurement hardware (multimeter, amplifier). That means that in fact all measuring methods are installed in one single setup, but the actual recordings are made serial with short temporal distances. The serialization of the measurement is realized by the use of a corresponding amount of reed switches, which sequentially connect and isolate the electrodes to be measured from the measuring circuits. The isolation is done galvanically and therefore prevents possible interferences between the different electrodes. The osmosis measurement is only made visually and is decoupled anyway. Fig. 5 shows a sketch of the switching setup. The relais are controlled by an Agilent 34901a 20 channel multiplexer. A second 34901a multiplexer is used as a data logger, which directs the measured signals to the internal multimeter of the multiplexer holding Agilent 34970A data acquisition unit.

The measurement duration of the individual data logger channels is approximately 200 ms due to an integration time of 10 net power line cycles (NPLC). That means that the two electric conductivity measurements and membrane potential measurements are made pseudo parallel with this temporal discrepancy of 200 ms. These pseudo parallel measurements are made every 10 s. Pictures recording the filling level are taken in (real) parallel every 10 min. The larger time interval is only due to the large data volumes of the pictures.

2.3. ODE model development

The measured transport phenomena taking place simultaneously are depicted in Fig. 6.

The ion transport is driven by the concentration gradient (Equation (1)). The opposite water transport is driven by the osmotic pressure difference, that also depends on the concentrations (Equation (3)). The rate determining coefficients are the salt diffusion coefficient D_S (coupled salt diffusion) and the solvent water permeability coefficient P_w. Fig. 6 illustrates this process.

The diffusive concentration change can be described by a simplified version of Fick's 2nd law:

$$\frac{dc}{dt} = D\frac{d^2c}{dx^2} \quad (1)$$

The concentration change in both of the diffusion cell chambers is assumed to be independent from an additional volume change. Thus, only the amount of substance n changes depending on the concentration gradient. The amount of substance change in both of the diffusion cell chambers, independent from an additional volume change, can therewith be described in form of a system of coupled differential equations:

$$\frac{dn_1}{dt} = -P_s/l(c_1 - c_2)$$
$$\frac{dn_2}{dt} = P_s/l\,(c_1 - c_2) \quad (2)$$

With $n_{1/2}$ being the amounts of substance in [mol] in the different cell chambers, P_s being the salt permeability coefficient in [m^2/s], l being the membrane thickness in [m] and $c_{1/2}$ being the concentrations in [mol/L]

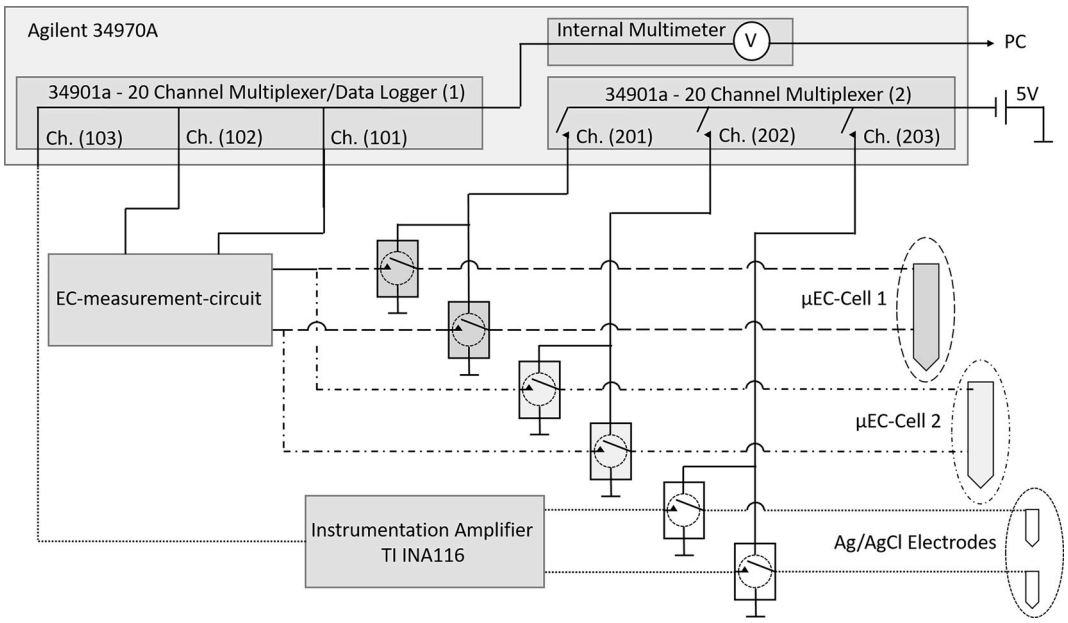

Fig. 5. Detailed switching setup for the serial, pseudo parallel measurements. The six reed switches are switched pairwise in an exclusive-OR manner, controlled by one Agilent 34970A multiplexer (ch. 201–203) that applies a control voltage of 5V. The measurement values are routed over another multiplexer to the internal multimeter (ch. 101–103). The µEC-cells 1 and 2 are switched separately (ch. 201 or ch. 202) but using the same measurement circuit alternately. The logged data from the EC measurement circuit therefore includes alternating the output signals of the two µEC-cells (ch. 102) and the corresponding input signal (ch. 101). The potential difference of the Ag/AgCl electrodes is switched by ch. 203 to the instrumentation amplifier and is recorded by ch. 103.

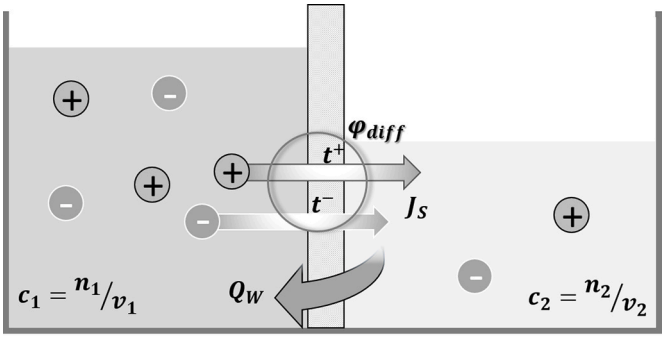

$$Substance\ Concentration: c = \frac{Amount\ of\ Substance\ n}{Solvent\ Volume\ v}$$

$$Salt\ Flux: J_S = -D_S\left(\frac{c_1 - c_2}{l}\right)$$

$$Water\ Flux: Q_W = P_W[2RT\left(\frac{c_1 - c_2}{l}\right)]$$

$$Diffusion\ Potential: \varphi_{diff} = \frac{RT}{F}\left(\frac{t^+}{z^+} - \frac{t^-}{z^-}\right) ln\left(\frac{c_1}{c_2}\right)$$

Fig. 6. Sketch of the transport processes taking place in parallel in the diffusion cell. The ion flux J_s is directed from the higher concentrated to the lower concentrated side, while the solvent flux Q_W is directed oppositely. Both fluxes depend on the concentration differences, which again depends on the fluxes. The rate determining coefficients are the salt and the permeability coefficients P_S and P_W. Additionally, a membrane potential can be measured if the apparent transport number of the involved ionic species in the membrane differ from each other.

on the higher- and on the lower concentrated side of the cell.

The osmosis caused volumetric water flux Q_W in $[m^3/m^2 s]$ can be described by:

$$\boldsymbol{Q_W = P \cdot (\sigma \Delta \Pi - p_{ext})} \quad 3$$

With P being the effective membrane permeance to water in [m/s Pa], $\Delta \Pi$ in [Pa] being the osmotic pressure difference, σ being a salt reflection coefficient (dimensionless) and p_{ext} being a counteracting pressure (e.g. hydrostatic pressure) in [Pa].

In the cell used here, however, the hydrostatic pressure is negligible compared to the osmotic pressure. A purely osmotic concentration balance would result in a maximum filling level difference of 2 cm. This results in a maximum hydrostatic pressure of 0.196 kPa. In contrast, the osmotic pressure difference can reach up to 2.4 MPa, with an initial concentration difference of 1:0.5 KCl. The salt reflection coefficient σ, which can be understood as coupled hydrodynamic frictional phenomena according to Kedem and Katchalsky [37], can also be neglected because the solution diffusion model used here assumes that the solvent and solute molecules permeate independently of each other and therefore convection and frictional coupling of fluxes can be neglected [12].

Following the solution diffusion model, according to Refs. [38–40] the effective permeance P, is then related to the actual water permeability P_W as follows:

$$\boldsymbol{P = \frac{P_W}{l}\frac{\rho_W V_W}{RT}} \quad 4$$

With ρ_W in $[g/m^3]$ being the density of water, V_w in $[g/mol]$ being the molar volume of water, l in $[m]$ being the membrane thickness and R and T having the usual physical meaning.

By inserting Equation (4) into Equation (3), some rearrangement and adding an eventual evaporation loss r_{evap} in [L/h], the resulting volume changes can be expressed as:

$$\frac{dv_1}{dt} = \frac{2P_W\rho_W V_W}{l}(c_1 - c_2) - r_{evap}$$
$$\frac{dv_2}{dt} = -\frac{2P_W\rho_W V_W}{l}(c_1 - c_2) - r_{evap} \quad 5$$

However, it is only possible to find a solution for the two previous presented systems of ODEs for concentration change (Equation (2)) and the volume change (Equation (5)) under the assumption of specific boundary conditions. The analytical solution for Equation (2) assumes a

constant volume and would therewith neglect an osmotic volume change, while the numerical solution for Equation (5) assumes a constant amount of substance (solute) and would therewith neglect the ion diffusion.

For an interdependent description of volume- and solute change, the two previous presented systems of ODEs which describe the concentration change (Equation (2)) and the volume change (Equation (5)) have to be summed up in one system of coupled ODE with four ODEs and four variables. The four variables result from the description of the concentration as a quotient of the amount of solute (n) and the amount of solvent (v):

$$c_x = \frac{n_x}{v_x} \tag{6}$$

The interdependent volume- and solute change can therewith be described by the following system of ODEs:

$$\begin{aligned} \frac{dn_1}{dt} &= -\frac{P_s}{l}\left(\frac{n_1}{v_1} - \frac{n_2}{v_2}\right) \\ \frac{dn_2}{dt} &= \frac{P_s}{l}\left(\frac{n_1}{v_1} - \frac{n_2}{v_2}\right) \\ \frac{dv_1}{dt} &= \frac{2P_w V_w}{l}\left(\frac{n_1}{v_1} - \frac{n_2}{v_2}\right) - r_{evap} \\ \frac{dv_2}{dt} &= -\frac{2P_w V_w}{l}\left(\frac{n_1}{v_1} - \frac{n_2}{v_2}\right) - r_{evap} \end{aligned} \tag{7}$$

To solve the system the initial volumes and amounts of substances in each chamber and the initial total amounts must be specified. Here, the total amount of substance n_{12} is constant over time while the total volume v_{12} decreases due to the evaporation losses, introduced in Equation (5):

$$v_{12} = v_1(0) + v_2(0), n_{12} = n_1(0) + n_2(0) \tag{8}$$

Further following substitutions are made:

$$\begin{aligned} \frac{n_1}{v_1} &= \frac{n_{12} - n_2}{v_{12} - v_2} \\ \frac{n_2}{v_2} &= \frac{n_{12} - n_1}{v_{12} - v_1} \end{aligned} \tag{9}$$

The actual solving is then done in python with the scipy.integrate.odeint function that solves a system of ordinary differential equations using lsoda from the FORTRAN library odepack [41].

However, this calculation is only valid if the electrolyte solution is assumed to be ideal. This only applies to solutions with infinite dilution, where interactions between the ionic species and the solvent can be excluded. At higher concentrations the interactions increase and the effective concentration (i.e. activity) must be considered. The deviation between concentration and activity is described by the activity coefficient (which is 1 for ideal solutions). Since the methods presented here are performed with non-ideal solutions, the activity coefficient must be taken into account. In the previous description of the ODE system, it is not given only for clarity. Actually, the activity coefficients are incorporated in form of a concentration dependent function. The function is composed of interpolated activity coefficients ranging from 0.0012 to 3.49 mol/kg. The data is taken from measurements published by Dash et al. [42].The concentration-describing terms n_x/v_x in the former descriptions are multiplied with the above mentioned function to obtain the actual activity:

$$\frac{n_x}{v_x} \cdot \mathrm{f}\left(\frac{n_x}{v_x}\right) = a_x \tag{10}$$

The apparent transport numbers, and hence the (perm)selectivity, can be directly calculated from the measured potential difference of the Ag/AgCl electrodes. The measured potential is the sum of the chloride dependent potential difference of the electrodes and the membrane potential. The overall potential can be written as:

$$\Delta E = -\frac{RT}{zF}\ln\frac{a_{1,Cl^-}}{a_{2,Cl^-}} - \frac{RT}{zF}(t_+ - t_-)\ln\frac{a_1}{a_2} \tag{11}$$

The diffusion potential is described by the second term of the equation. It is caused by the differences in electrical mobility of the individual ions. The differences are expressed by the apparent transport numbers $t^{+/-}$, which indicate the individual share of the ions on the total electric current.

In short, the ions could have different velocities when they enter a phase boundary.

Therefore, the ion fluxes have to be regarded separately and even without an external electric field the migration term has to be involved:

$$J_i = -D_i\left(\frac{dc_i}{dx} - \frac{z_i F}{RT}c_i\frac{d\varphi}{dx}\right) \tag{12}$$

If one of the ionic species hurries ahead of its counter ions an electric field will build up. This field pulls back the faster ionic species proportional to the distance to its counter ions and likewise drags the slower ions toward the faster ones. In the quasi steady state the electric field has a defined value that results in equal transport velocities for the ionic species c_i.

With the Poisson equation the electric potential is calculated from the charge density ρ that results from the movement of the ionic species [43]:

$$\frac{dE}{dx} = \frac{\rho}{\varepsilon};\ \rho = F\sum_i z_i c_i \tag{13}$$

The resulting local electrical field $E = d\varphi/dx$ reciprocally influences the movement of the ions.

The resulting potential difference, which is measurable over the membrane is then the diffusion potential. It can also be derived from a more thermodynamically point of view leading to the second term declared in Equation *11*.

The apparent transport numbers can then be determined with the knowledge of the initial electrolyte concentrations and the measured potential difference from the overall measured potential (Equation *11*), which can be rearranged with $t^+ + t^- = 1$ to:

$$t^+_{mem} = -\frac{\Delta E + \frac{RT}{F}\ln\left(\frac{a_{1,Cl^-}}{a_{2,Cl^-}}\right) - \frac{RT}{F}\ln\left(\frac{a_1}{a_2}\right)}{2\frac{RT}{F}\ln\left(\frac{a_1}{a_2}\right)} \tag{14}$$

Furthermore, it is assumed that the initial diffusion potential has already been formed when the measurements start. The settlement of the diffusion potential is recognizable for $t^+ \gg t^-$ by reaching a global maximum after a short initial increase of potential, and for $t^- \gg t^+$ by going through a saddle point after a fast initial potential decrease. This assumption is made due to the relatively short time span of the initial potential formation, and the time lag between the filling of the cell and start of measurement. Moreover, no increase in potential is measurable at the start of the actual measurement ($t^+ \gg t^-$).

This procedure can however lead to a slight underestimation of the apparent transport number, if the time lag between cell preparation and start of measurement takes too long. Ideally, the extreme value is just recognizable.

3. Results and discussion

All measurements are made at a stable laboratory ambient temperature of 21 °C and humidity of 30%.

All measurements are performed with a KCl solution. The initial concentrations in all measurements have a ratio of 2:1 (1:0.5 M, 2:1 M).

The simultaneously measured concentration change and volume change in both cell chambers with an electrolyte concentrations of 1 M and 0.5 M is depicted in Fig. 7. The simultaneously measured potential difference over the membrane is depicted in Fig. 8.

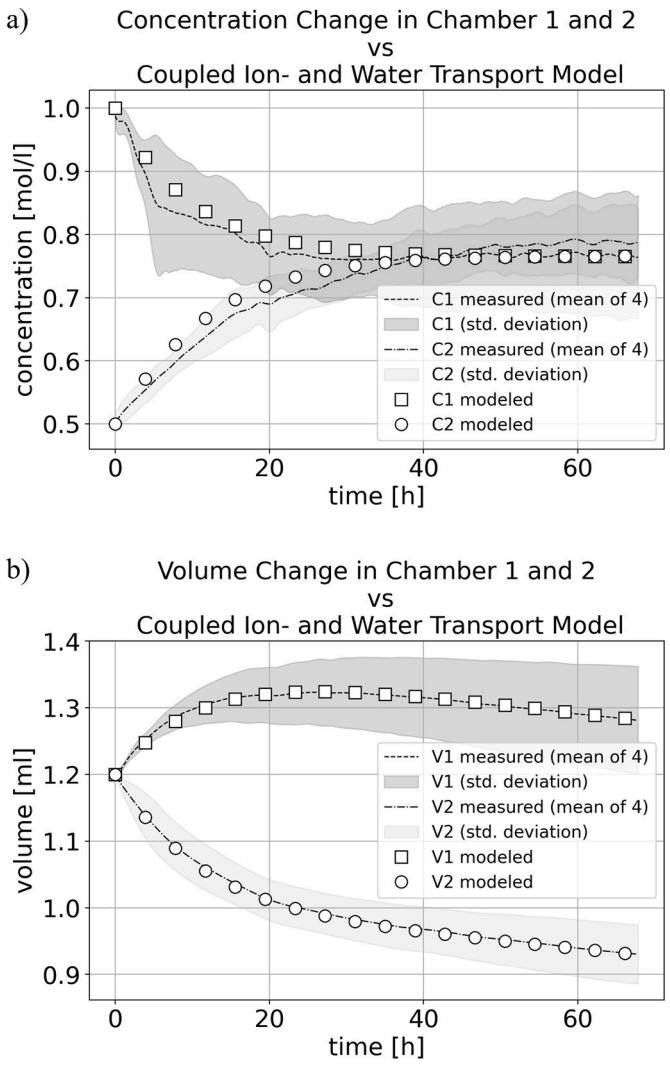

Fig. 7. (a) Concentration change measurement results in comparison to theoretical concentration courses and (b) the coupled volume change model in comparison to the measured volume change. The modeled courses (□ 1 M start concentration, ○ 0.5 M start concentration) are calculated by solving system of coupled ODEs which includes the solute transport (diffusion) as well as the solvent transport (osmosis).

Fig. 7 (a) displays the change of concentration in both chambers, determined by EC measurements and Fig. 7 (b) presents the osmosis driven volume change also in both chambers. The dashed lines (– –) in Fig. 7 (a) and (b) are representing the measured changes of the higher concentrated cell side (1 M), accordingly the pointed-dashed lines (– • –) are representing the changes of the lower concentrated side (0.5 M). Fig. 8 shows the measured potential difference between the two Ag/AgCl electrodes. The potential consists of the concentration dependent electrode potentials and the membrane potential.

3.1. Coupled ion diffusion and osmosis

The ions diffuse from the higher to the lower concentrated solution. Simultaneously the opposite directed water transport accelerates the equalization as well by diluting the higher concentrated side and likewise concentrating the lower concentrated side. Since both mechanisms depend on the concentration gradient, they also have to be modeled interdependently.

The presented model allows the determination of the membrane transport coefficients P_S and P_w under consideration of the coupled

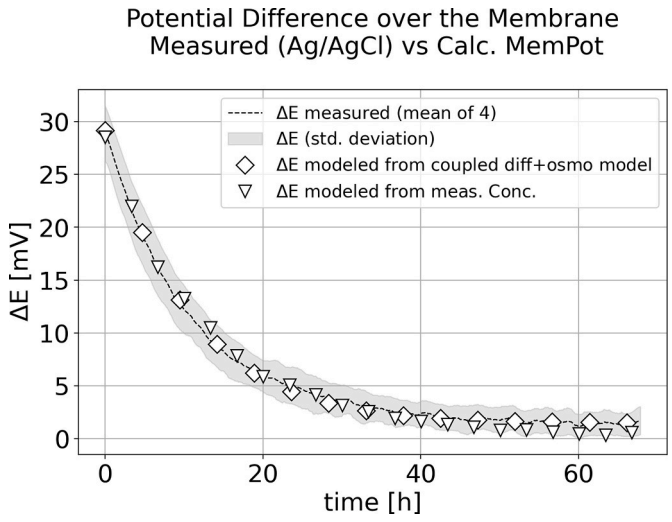

Fig. 8. Potential difference of the two Ag/AgCl electrodes measures over the membrane in comparison with the calculated potential difference. ▽: calculated from the measured concentration change. ⋄: Calculated from the coupled diffusion-osmosis model.

dependency of the concentration change from the diffusive solute transport and the osmotic solvent transport. The transport coefficients are determined by varying the transport coefficients in the diffusion- and osmosis-coupled model (Equation (7)) and thereby fitting the modeled curves to the measured ones. Fig. 7 shows concentration- and volume change measurement in comparison to modeled curves.

The transport coefficients for 1:0.5 M KCl resulting from the fitting are: $P_S = 3.25 \cdot 10^{-12} m^2/s \left(\pm 2.5 \cdot 10^{-13}\, m^2/s \right)$ and $P_W = 1.03 \cdot 10^{-10} m^2/s \left(\pm 2.07 \cdot 10^{-12}\, m^2/s \right)$. These values are in agreement with general values from the literature ($P_S = 1 \cdot 10^{-13} \ldots 1 \cdot 10^{-11} m^2/s$ and $P_W = 1 \cdot 10^{-11} \ldots 2 \cdot 10^{-10} m^2/s$ [39]).

The diffusion coefficients can only be estimated, since the actual partitioning coefficients are unknown.

According to the comparison of different IEMs made by Kingsbury et al. [39] the salt partitioning coefficient K_S is in a range between $0.05 - 0.24$ and the water uptake K_W is in a range between $0.1 - 0.33$.

Following to the solution diffusion theory the diffusion coefficient can be calculated as the quotient of the permeability coefficient and the partitioning coefficient:

$$\boldsymbol{D_{S,W} = P_{S,W} / K_{S,W}} \qquad 15$$

This results in a salt diffusion coefficient $D_S = 1.35 \cdot 10^{-11} - 6.5 \cdot 10^{-11} m^2/s$ and a water diffusion coefficient $D_W = 3.12 \cdot 10^{-10} - 1.03 \cdot 10^{-9} m^2/s$. These results are also in agreement with [39].

In comparison, the transport coefficients are higher for the coupled ion diffusion- and osmosis-driven concentration change, than the transport coefficients for the concentration change driven solely by diffusion or osmosis. Consequently, the rate determining coefficients will be overestimated if they are investigated separately.

In addition, measurements were made with higher concentrations of 2:1 mol. This serves to verify whether the method is generally also applicable with other concentrations. The transport parameters determined during these measurements are $P_W = 1.0 \cdot 10^{-10} m^2/s \left(\pm 0.82 \cdot 10^{-12}\, m^2/s \right)$, $P_S = 4.5 \cdot 10^{-12} m^2/s \left(\pm 7.07 \cdot 10^{-13}\, m^2/s \right)$ and $t^+ = 0.89$ (± 0.017). Table 1 shows the values once again in comparison with the values for the measurement with 1:0.5 M KCl and the comparable literature values. There are no significant deviations between the values determined here. The method can therefore be considered stable in a range of at least 0.5–2 M, with a ratio of 2:1.

Table 1
Comparison of the Nafion® NR211 transport parameters determined in this work with concentration gradients of 1:0.5 M KCl and 2:1 M KCl, and the literature values.

Conc. Gradient [Membrane]	P_S (m^2/s)	P_W (m^2/s)	t^+
1:0.5 M KCl [Nafion® NR211]	$(3.25 \pm 0.25)\cdot10^{-12}$	$(1.03 \pm 0.021)\cdot10^{-10}$	0.863 ± 0.0805
2:1 M KCl [Nafion® NR211]	$(4.5 \pm 0.707)\cdot10^{-12}$	$(1.0 \pm 0.082)\cdot10^{-10}$	0.907 ± 0.0171
Lit. Val. div. [IEM div.]	$1\cdot10^{-13}$…$1\cdot10^{-11}$ [39]	$1\cdot10^{-11}$…$2\cdot10^{-10}$ [39]	0.765 … 0.995 [23, 35,44]

3.2. Membrane potential measurement

The measured potential difference of the Ag/AgCl electrodes over the membrane is shown in Fig. 8. From the measured potential difference value and with the knowledge of the initial concentrations, the apparent transport numbers t^+ is determined by using Equation (14). The apparent transport number for 1:0.5 M KCl is $t^+ = 0.863$ (±0.0805) and $t^+ = 0.907$ (±0.0171) for 2:1 M KCl. These values are in accordance to other literature values for KCl in Nafion®. Literature values ranging from $t^+ = 0.80$–0.90 depending on the membrane thickness [23], and $t^+ = 0.88$–0.984 depending on the concentration [35]. Apparent transport numbers for NaCl in other IEM are ranging from $t^+ = 0.765$–0.995 depending on the concentration [22].

According to Ref. [35] the apparent transport number t^+ decreases with increasing concentration (1 N KCl: $t^+ = 0.888$; 0.1 N KCl: $t^+ = 0.984$). This observation is in contrast to other observations [22], where the apparent counter ion transport number t^+ increases with increasing concentration. The difference in observations might be due to the methods used to determine the transport number. Stenina et al. [35] calculated the transport number from the individual diffusion coefficients leading to a decreasing counter ion transport number with increasing ion concentration, while Cha et al. [22] determined the transport number from membrane potential measurements leading to an increasing counter ion transport with increasing concentration.

The actual reason for this differences is currently unknown to the authors. However, the later approach is similar to the one presented in this work and shows a similar trend concerning the increase of the transport number with increasing concentration.

The slightly lower apparent transport number determined in this work in contrast to the results from Cha et al. [22] might be due to an underestimation of the apparent transport number, which was already mentioned in the experimental section. An underestimation can be caused by a time delay between the filling of the cell and the actual start of the measurement. This leads to the consequence that the membrane potential is no longer measured at the maximum, but already at the drop.

With the apparent transport numbers and the known concentration propagation over time it is further possible to model the complete course of the potential differences over time by using Equation (11). Fig. 8 shows the measured potential difference in comparison to two modeled potential differences, $\bigtriangledown$ is calculated by using the EC measured concentration change and $\diamond$is calculated by using the concentration change modeled with Equation (7).

The coefficients determined with the approach presented in this work are in agreements with the values determined in other works. All the individual measuring methods employed in this work have been used before in similar double chamber setups [8–12,16,20,23,25].

In difference to these works, the main coefficients are all determined simultaneously in one setup. Additionally, special attention is put on the coupling of diffusive ion transport and osmotic water transfer. Even though it was practically investigated by others in a similar approach, their theoretical basis were just simplifications for one specific case that assumed a constant volume over time [45], or the measurements were not automated and required a high effort of individual manual measurements [46].

The worked-out mathematical description of coupled and dependent transport phenomena enables a determination of the coefficients by fitting the models to the measurements. The slight differences between the measurements and the fitted courses might be due to inaccuracies during the measurements. First, the unexpected loss of volume could not be determined properly and had to be estimated. Second, the measured values of the homemade μEC electrodes tend to drift. This can lead to inaccuracies in the concentration measurements (visible in Fig. 6a). The reason for that drift is that the degree of platinization of the electrodes can decrease over time, leading to a decrease in the surface area and thus to a deviation from the reference value. Finally, the optical filling height recording is sensitive to light influences from the surrounding.

Nevertheless, reproducible measurements on Nafion® have shown how the synchronous measurement and determination of the coupled transport parameters salt diffusion coefficient, water permeability coefficient and the apparent transport numbers can be done. Therefore the concentration change, the volume change and the membrane potential have to be measured.

It would also be possible to vary the measurement methods according to the situation. Instead of the sensitive EC measurements, an additional single junction reference electrode per side could be used. This would allow the determination of the chloride concentration by measuring it directly against the junctionless Ag/AgCl electrode. In addition, the membrane potential could be measured directly by measuring the two junction reference electrodes against each other. However, a possible drawback of this approach would be the possibility of distortion of the electrolyte concentrations due to leakage at the junction. This is a problem that should not be neglected, especially in the case of long-term measurements.

The determined coefficients, however, are just the “external” accessible parameters of the membrane. That means, the membrane under investigation is a black box from the here presented experimental point of view. No details of the inside can be explored to learn more about the internal processes of the membrane. One additional method could therefore be molecular dynamics simulation (MDS). MDS allows a study of the local intermolecular interactions in the nano-scale.

For example, with MDS it is possible to investigate the water sorption influence on the molecular structure and alignment [47] and therewith the ion transport mechanisms in dependence on the hydration [48].

FEM simulation on the other hand allows a more global analysis of the inner membrane distribution of the ions, for example in the form of diffusion profiles [49]. The System of ODEs presented in this work together with the work of Sokalski et al. [43], concerning the solution of the Nernst Planck Poisson equations, could be a starting point for a FEM model of the ion distribution inside IEMs.

4. Conclusion

A method for the simultaneous determination of transport coefficients of aqueous electrolyte solution in polymers was successfully developed. These coefficients are the salt diffusion coefficient D_S, the water permeability coefficient P_W and the apparent transport numbers t^+ and t^-.

The method is based on a practical measurement setup and an ODE model. The measurement setup consists of a diffusion cell with the possibility for parallel measurements of the concentration change, the volume change and the membrane potential. The actual transport coefficients are determined by adjusting the corresponding model parameters so that the theortical curves are fitted to the measurements. The model consists of a system of coupled ODEs, which is solved numerically. The method was validated by determining the transport

properties of a Nafion® NR211 ion exchange membrane. The properties are shown in Table 1.

The presented simultaneous measurement method therewith contributes to the field of characterization and comparison of different materials, in the way that it enables a more holistic view of the transport phenomena and further enables the identification of the dominant phenomena.

Author statement

Lars Varain: Research & Investigation, Idea & Conceptualization, Data Curation, Analysis, Software and Simulation, Original Draft Preparation, Revise & Editing.

Günter Fafilek: Supervision, Idea & Conceptualization, Verification.

Michael Nelhiebel: Funding Acquisition.

Silvia Larisegger: Project Administration, Funding Acquisition.

Declaration of competing interest

The authors declare that they have no known competing financial interests or personal relationships that could have appeared to influence the work reported in this paper.

Data availability

Data will be made available on request.

Acknowledgement

The author gratefully acknowledges the financial support funded by the Austrian Research Promotion Agency (FFG, Project No. 898207).

References

[1] J. Luo, C. Wu, T. Xu, Y. Wu, Diffusion dialysis-concept, principle and applications, J. Membr. Sci., Bd. 366 (Nr. 1) (Jan. 2011) 1–16, https://doi.org/10.1016/j.memsci.2010.10.028.

[2] T. Scarazzato u.a., Chapter 5 - achievements in electrodialysis processes for wastewater and water treatment, in: A. Basile, K. Ghasemzadeh Hrsg (Eds.), Current Trends and Future Developments on (Bio-) Membranes, Elsevier, 2020, pp. 127–160, https://doi.org/10.1016/B978-0-12-817378-7.00005-7.

[3] M. Fidaleo, M. Moresi, Electrodialysis applications in the food industry, in: Advances in Food and Nutrition Research, Academic Press, 2006, pp. 265–360, https://doi.org/10.1016/S1043-4526(06)51005-8.

[4] F. Hell, J. Lahnsteiner, The application of electrodialysis for drinking water treatment, in: H. Rubin, U. Shamir, P. Nachtnebel, J. Fürst Hrsg (Eds.), Water Resources Quality: Preserving the Quality of Our Water Resources, Springer, Berlin, Heidelberg, 2002, pp. 315–327, https://doi.org/10.1007/978-3-642-56013-2_18.

[5] A.H. Avci, R.A. Tufa, E. Fontananova, G. Di Profio, E. Curcio, Reverse Electrodialysis for energy production from natural river water and seawater, Energy, Bd. 165 (Dez. 2018) 512–521, https://doi.org/10.1016/j.energy.2018.09.111.

[6] E. Mercer u.a., Hybrid membrane distillation reverse electrodialysis configuration for water and energy recovery from human urine: an opportunity for off-grid decentralised sanitation, J. Membr. Sci., Bd. 584 (Aug. 2019) 343–352, https://doi.org/10.1016/j.memsci.2019.05.010.

[7] J.G. Wijmans, R.W. Baker, The solution-diffusion model: a review, J. Membr. Sci., Bd. 107 (1) (Nov. 1995) 1–21, https://doi.org/10.1016/0376-7388(95)00102-I.

[8] W. Pusch, Chapter 1.4 Measurement techniques of transport through membranes, Desalination, Bd. 59 (Aug. 1986) 105–198, https://doi.org/10.1016/0011-9164(86)90028-7.

[9] G.M. Geise, B.D. Freeman, D.R. Paul, Characterization of a sulfonated pentablock copolymer for desalination applications, Polymer, Bd. 51 (24) (Nov. 2010) 5815–5822, https://doi.org/10.1016/j.polymer.2010.09.072.

[10] G.M. Geise, B.D. Freeman, D.R. Paul, Sodium chloride diffusion in sulfonated polymers for membrane applications, J. Membr. Sci., Bd. 427 (Jan. 2013) 186–196, https://doi.org/10.1016/j.memsci.2012.09.029.

[11] J. Kamcev, E.-S. Jang, N. Yan, D.R. Paul, B.D. Freeman, Effect of ambient carbon dioxide on salt permeability and sorption measurements in ion-exchange membranes, J. Membr. Sci., Bd. 479 (Apr. 2015) 55–66, https://doi.org/10.1016/j.memsci.2014.12.031.

[12] R.S. Kingsbury, S. Zhu, S. Flotron, O. Coronell, Microstructure determines water and salt permeation in commercial ion-exchange membranes, ACS Appl. Mater. Interfaces, Bd. 10 (46) (Nov. 2018) 39745–39756, https://doi.org/10.1021/acsami.8b14494.

[13] B. Craster, T.G.J. Jones, Permeation of a range of species through polymer layers under varying conditions of temperature and pressure: in situ measurement methods, Polymers, Bd 11 (6) (Juni 2019), https://doi.org/10.3390/polym11061056. Art. Nr. 6.

[14] H. Ohshima, T. Kondo, Membrane potential and Donnan potential, Biophys. Chem., Bd. 29 (3) (Apr. 1988) 277–281, https://doi.org/10.1016/0301-4622(88)85049-X.

[15] T. Sokalski, A. Lewenstam, Application of Nernst–Planck and Poisson equations for interpretation of liquid-junction and membrane potentials in real-time and space domains, Electrochem. Commun., Bd. 3 (3) (März 2001) 107–112, https://doi.org/10.1016/S1388-2481(01)00110-2.

[16] H. Yasuda, C.E. Lamaze, L.D. Ikenberry, Permeability of solutes through hydrated polymer membranes. Part I. Diffusion of sodium chloride, Makromol. Chem., Bd. 118 (1) (1968) 19–35, https://doi.org/10.1002/macp.1968.021180102.

[17] Q. Duan, H. Wang, J. Benziger, Transport of liquid water through Nafion membranes, J. Membr. Sci., Bd. 392–393 (März 2012) 88–94, https://doi.org/10.1016/j.memsci.2011.12.004.

[18] P. Majsztrik, A. Bocarsly, J. Benziger, Water permeation through nafion membranes: the role of water activity, J. Phys. Chem. B, Bd. 112 (51) (Dez. 2008) 16280–16289, https://doi.org/10.1021/jp804197x.

[19] W. Grot, 9 - experimental methods, in: W. Grot Hrsg (Ed.), Fluorinated Ionomers, second ed., Plastics Design Library. William Andrew Publishing, 2011, pp. 211–233, https://doi.org/10.1016/B978-1-4377-4457-6.10009-3.

[20] G.M. Geise, H.J. Cassady, D.R. Paul, B.E. Logan, M.A. Hickner, Specific ion effects on membrane potential and the permselectivity of ion exchange membranes, Phys. Chem. Chem. Phys., Bd. 16 (39) (Sep. 2014) 21673–21681, https://doi.org/10.1039/C4CP03076A.

[21] P.A. Sosa-Fernández, J.W. Post, H.L. Nabaala, H. Bruning, H. Rijnaarts, Experimental evaluation of anion exchange membranes for the desalination of (waste) water produced after polymer-flooding, Membranes, Bd. 10 (11) (Nov. 2020), https://doi.org/10.3390/membranes10110352. Art. Nr. 11.

[22] J.-E. Cha, M.H. Seo, Y.-W. Choi, W.B. Kim, A practical approach to measuring the ion-transport number of cation-exchange membranes: effects of junction potential and analyte concentration, J. Membr. Sci., Bd. 635 (Okt. 2021), 119471, https://doi.org/10.1016/j.memsci.2021.119471.

[23] M.A. Izquierdo-Gil, V.M. Barragán, J.P.G. Villaluenga, M.P. Godino, Water uptake and salt transport through Nafion cation-exchange membranes with different thicknesses, Chem. Eng. Sci., Bd. 72 (Apr. 2012) 1–9, https://doi.org/10.1016/j.ces.2011.12.040.

[24] A. Zlotorowicz, R.V. Strand, O.S. Burheim, Ø. Wilhelmsen, S. Kjelstrup, The permselectivity and water transference number of ion exchange membranes in reverse electrodialysis, J. Membr. Sci., Bd. 523 (Feb. 2017) 402–408, https://doi.org/10.1016/j.memsci.2016.10.003.

[25] M. Fernández de Labastida, A. Yaroshchuk, Transient membrane potential after concentration step: a new method for advanced characterization of ion-exchange membranes, J. Membr. Sci., Bd. 585 (Sep. 2019) 271–281, https://doi.org/10.1016/j.memsci.2019.05.012.

[26] C.H. Hamann, W. Vielstich, Elektrochemie, 4., Vollständig überarbeitete und Aktualisierte Auflage, Wiley-VCH-Verlag GmbJ &Co. KGaA, Weinheim, 2005.

[27] B.L. Werkhoven, R. van Roij, Coupled water, charge and salt transport in heterogeneous nano-fluidic systems, Soft Matter, Bd. 16 (6) (Feb. 2020) 1527–1537, https://doi.org/10.1039/C9SM02144B.

[28] A. Narębska, S. Koter, W. Kujawski, Ions and water transport across charged nafion membranes, Irreversible thermodynamics approach", Desalination, Bd. 51 (1) (Jan. 1984) 3–17, https://doi.org/10.1016/0011-9164(84)85048-1.

[29] Nafion NR211 and NR212 Ion Exchange Materials Solution Cast Membranes, Chemours, 2021 [Online]. Verfügbar unter: https://www.chemours.com/en/-/media/files/nafion/nafion-nr211-nr212-p-11-product-info.pdf.

[30] J. Kamcev, D.R. Paul, B.D. Freeman, Ion activity coefficients in ion exchange polymers: applicability of Manning's counterion condensation theory, Macromolecules, Bd. 48 (21) (Nov. 2015) 8011–8024, https://doi.org/10.1021/acs.macromol.5b01654.

[31] R. Sujanani, L.E. Katz, D.R. Paul, B.D. Freeman, Aqueous ion partitioning in Nafion: applicability of Manning's counter-ion condensation theory, J. Membr. Sci., Bd. 638 (Nov. 2021), 119687, https://doi.org/10.1016/j.memsci.2021.119687.

[32] G.M. Geise, L.P. Falcon, B.D. Freeman, D.R. Paul, Sodium chloride sorption in sulfonated polymers for membrane applications, J. Membr. Sci., Bd. 423–424 (Dez. 2012) 195–208, https://doi.org/10.1016/j.memsci.2012.08.014.

[33] F. Xu, S. Leclerc, D. Stemmelen, J.-C. Perrin, A. Retournard, D. Canet, Study of electro-osmotic drag coefficients in Nafion membrane in acid, sodium and potassium forms by electrophoresis NMR, J. Membr. Sci., Bd. 536 (Aug. 2017) 116–122, https://doi.org/10.1016/j.memsci.2017.04.067.

[34] R. Lteif, L. Dammak, C. Larchet, B. Auclair, Conductivitéélectrique membranaire: étude de l'effet de la concentration, de la nature de l'électrolyte et de la structure membranaire, Eur. Polym. J., Bd. 35 (7) (Juli 1999) 1187–1195, https://doi.org/10.1016/S0014-3057(98)00213-4.

[35] I.A. Stenina, Ph Sistat, A.I. Rebrov, G. Pourcelly, A.B. Yaroslavtsev, Ion mobility in Nafion-117 membranes, Desalination, Bd. 170 (1) (Okt. 2004) 49–57, https://doi.org/10.1016/j.desal.2004.02.092.

[36] P.J. Brewer, R.J.C. Brown, Effect of structural design of silver/silver chloride electrodes on stability and response time and the implications for improved accuracy in pH measurement, Sensors, Bd. 9 (1) (Jan. 2009) 118–130, https://doi.org/10.3390/s90100118.

[37] O. Kedem, A. Katchalsky, A physical interpretation of the phenomenological coefficients of membrane permeability, J. Gen. Physiol., Bd. 45 (1) (Sep. 1961) 143–179.

[38] A.A. Merdaw, A.O. Sharif, G.A.W. Derwish, „Water permeability in polymeric membranes, Part I“, Desalination, Bd 260 (1) (Sep. 2010) 180–192, https://doi.org/10.1016/j.desal.2010.04.042.

[39] R.S. Kingsbury, J. Wang, O. Coronell, Comparison of water and salt transport properties of ion exchange, reverse osmosis, and nanofiltration membranes for desalination and energy applications, J. Membr. Sci., Bd. 604 (Juni 2020), 117998, https://doi.org/10.1016/j.memsci.2020.117998.

[40] G.M. Geise, D.R. Paul, B.D. Freeman, Fundamental water and salt transport properties of polymeric materials, Prog. Polym. Sci., Bd. 39 (1) (Jan. 2014) 1–42, https://doi.org/10.1016/j.progpolymsci.2013.07.001.

[41] ODE Solver, scipy.integrate.odeint, 17, Juni 2021. https://docs.scipy.org/doc/scipy/reference/generated/scipy.integrate.odeint.html.

[42] D. Dash, S. Kumar, C. Mallika, U.K. Mudali, „NewData on Activity Coefficients of Potassium , Nitrate , and Chloride Ions in Aqueous Solutions of KNO 3 and KCl by Ion Selective Electrodes“, 2015. Zugegriffen: 8. Februar 2023. [Online]. Verfügbar unter: https://www.semanticscholar.org/paper/NewData-on-Activity-Coefficients-of-Potassium-%2C-%2C-3-Dash-Kumar/7e5ffaf9bccc947fb96771380bab5eca5f7ed094.

[43] T. Sokalski, P. Lingenfelter, A. Lewenstam, Numerical solution of the coupled Nernst−Planck and Poisson equations for liquid junction and ion selective membrane potentials, J. Phys. Chem. B, Bd. 107 (11) (2003) 2443–2452, https://doi.org/10.1021/jp026406a. März.

[44] A. Lehmani, P. Turq, M. Périé, J. Périé, J.-P. Simonin, Ion transport in Nafion® 117 membrane, J. Electroanal. Chem., Bd. 428 (Nr. 1) (1997) 81–89, https://doi.org/10.1016/S0022-0728(96)05060-7. Mai.

[45] M.A. Izquierdo-Gil, J.P.G. Villaluenga, S. Muñoz, V.M. Barragán, The correlation between the water content and electrolyte permeability of cation-exchange membranes, Int. J. Mol. Sci., Bd. 21 (16) (2020), https://doi.org/10.3390/ijms21165897. Aug.

[46] G.H. Lopes, N. Ibaseta, P. Guichardon, How can osmosis and solute diffusion be coupled for the simultaneous measurement of the solvent and solute permeabilities of membranes? Desalination, Bd. 387 (2016) 61–74, https://doi.org/10.1016/j.desal.2016.03.006. Juni.

[47] E. Sireci, G. De Luca, J. Luque Di Salvo, A. Cipollina, G. Micale, Prediction of equilibrium water uptake and ions diffusivities in ion-exchange membranes combining molecular dynamics and analytical models, J. Membr. Sci., Bd. 668 (Feb. 2023), 121283, https://doi.org/10.1016/j.memsci.2022.121283.

[48] J. Luque Di Salvo, G. De Luca, A. Cipollina, G. Micale, Effect of ion exchange capacity and water uptake on hydroxide transport in PSU-TMA membranes: a DFT and molecular dynamics study, J. Membr. Sci., Bd. 599 (Apr. 2020), 117837, https://doi.org/10.1016/j.memsci.2020.117837.

[49] V. Ionescu, Numerical modeling of a desalination process through the ion-exchange membranes of a electrodialysis cell, in: L. Moldovan, A. Gligor, Hrsg (Eds.), The 16th International Conference Interdisciplinarity in Engineering, Springer International Publishing, Cham, 2023, pp. 803–814, https://doi.org/10.1007/978-3-031-22375-4_65, in Lecture Notes in Networks and Systems.